Scalable Semi-Batch Synthesis of Cellulose Nanocrystal–Polyvinyl Acetate Nanocomposites for Industrial Applications

Advances in Polymer Technology

WILEY

RESEARCH ARTICLE OPEN ACCESS

Scalable Semi-Batch Synthesis of Cellulose Nanocrystal–Polyvinyl Acetate Nanocomposites for Industrial Applications

Shahab Nasr[1] | Pooria Khalili[1] | Juliana Aristéia de Lima[1,2] | Fathi Gouda[1] | Gunnar Westman[3] | Mikael Skrifvars[1]

[1]Swedish Centre for Resource Recovery, University of Borås, Borås 50190, Sweden | [2]Department of Polymer, Fiber and Composite, RISE Research Institutes of Sweden, Borås, Sweden | [3]Chalmers University of Technology, Gothenburg 41296, Sweden

Correspondence: Shahab Nasr (shahab.nasr@hb.se)

Received: 18 June 2025 | **Revised:** 19 March 2026 | **Accepted:** 19 March 2026

Academic Editor: Srijoni Sengupta

Keywords: cellulose nanocrystals | nanocomposites | polyvinyl acetate latex | semi-batch emulsion polymerization

ABSTRACT

This study reports the synthesis of a stable and homogeneous nanocomposite of cellulose nanocrystals (CNCs) and vinyl acetate (VA) monomer via a semi-batch water-based emulsion polymerization technique, targeting a total solid content (TSC) of 50 wt.% to meet industrial requirements such as smaller storage volume, and easier transportation. The semi-batch approach enabled a consistent distribution of the reactants and improved scalability for industrial applications. CNCs were successfully incorporated into a polyvinyl acetate (PVAc) latex formulation at concentrations of up to 3.22 wt.% relative to VA monomer. Fourier-transform infrared spectroscopy indicated the consumption of hydroxyl groups on the CNC surfaces. The nanocomposites containing 1.93% CNC demonstrated the most promising performance, reducing the water sensitivity of pristine PVAc and lowering both the water vapor transmission rate (WVTR) and permeation. Nevertheless, the increased CNC content induced an uneven surface topography and a broader polymer particle size and distribution, as observed by polarized light and scanning electron microscopy. Mechanical testing revealed a general reduction in the tensile properties relative to neat PVAc, although the 1.93 wt. % CNC sample exhibited the least decline. The resulting nanocomposites exhibited an extended shelf life and colloidal stability, indicating their potential for industrial applications.

1 | Introduction

Nanoparticles are increasingly acknowledged for their ability to enhance the properties and functionalities of polymer composites [1–6]. Initially, nanocomposite development started by using inorganic nanoparticles; however, increasing environmental concerns have shifted attention towards organic and sustainable alternatives [7–9]. Among these, CNCs, which are bio-based nanoparticles obtained via acid hydrolysis, have gained significant interest due to unique characteristics [10, 11]. Their sustainability, favorable mechanical parameters and abundance of surface hydroxyl groups make them particularly attractive for modification of polymers [12]. Their incorporation into polymer matrices has been generally found to enhance thermo-mechanical performance and reduce water sensitivity while maintaining biodegradability [13]. These enhancements are primarily attributed to the formation of hydrogen bonds with hydroxyl groups on the surface of the CNCs, facilitating the formation of a percolated network, which can act as reinforcement [14]. A challenge is the hydrophilic nature of CNCs and their tendency to self-aggregate via hydrogen bonding, which can lead to stress-concentrated

areas in the nanocomposite and can compromise the homogeneity of the resulting products [15].

The extraction of CNCs using sulfuric acid hydrolysis introduces a negative charge onto the CNC particles, which is advantageous for preparing stable aqueous suspensions owing to enhanced electrostatic repulsion forces [16]. Enhancing the properties of water-based polymers using CNCs may be more straightforward than using other polymers, as water serves as a medium that facilitates their dispersion and interaction. The hydrophilic nature of CNCs enables easier dispersion, especially when CNCs are incorporated during the polymerization process [17].

Recent investigations of nanocellulose-reinforced waterborne latex systems have predominantly focused on acrylic-based copolymers. For instance, carboxylated cellulose nanocrystals (CNCs) have been incorporated into butyl acrylate/methyl methacrylate and acrylic acid–containing latex formulations [18, 19]. Comprehensive discussions are available in recent reviews addressing nanocellulose in heterogeneous polymer systems [20]. In contrast, studies specifically targeting polyvinyl acetate (PVAc)/CNC systems remain scarce. Earlier studies have reported solution-cast PVAc/CNC nanocomposites [21] and crosslinked PVAc/CNC systems prepared via in situ polymerization [22]. Although similar approaches have been reported previously, they were conducted at low TSC, limiting their relevance for industrial applications [22, 23]. PVAc in latex form is considered as a green polymer due to low energy consumption during the synthesis, simplicity of production, and low toxicity [24]. The merit of PVAc for manufacturing nanocomposites with CNCs have been previously reported by Geng et al. [22]. Although it is possible to incorporate CNCs into PVAc latexes either through in situ polymerization or post-addition to the latex, in situ addition showed more promising results [23].

In our previous research [6], we investigated the use of CNC-modified PVAc nanocomposite latexes as a matrix in viscose-fabric reinforced laminates and assessed the mechanical performance for the composites. The matrices were synthesized via semi-batch emulsion polymerization and subsequently applied to viscose fabrics using a hand-layup prepreg technique followed by compression molding to produce composite laminates. The results showed that the incorporation of CNCs, particularly at an optimal loading of 1.2 wt.%, significantly improved the mechanical performance and structural integrity of the composites, leading to a 13.7% increase in ultimate tensile strength and a 36.2% increase in impact resistance, along with improvements in flexural and interlaminar shear strength. Although the CNC-modified matrices generally exhibited a lower elastic modulus, they provided higher ductility, with the elongation at break increasing by up to 31.5%. However, at higher CNC loadings, the performance tended to decline, mainly owing to CNC agglomeration and processing limitations, such as increased viscosity and air bubble entrapment.

In contrast, the current study focuses on the synthesis of the latex as the primary product, establishing a scalable semi-batch emulsion polymerization method to produce high–total-solid-content (~50 wt. %) PVAc/CNC nanocomposite latexes capable of forming films. The aim has been to systematically examine the relationship between CNC incorporation and the microstructure of the formed films, as well as coating-relevant properties such as wettability, water vapor transmission rate (WVTR), thermal behavior, and tensile response. Consequently, this study contributes to the scalable synthesis and characterization of latex/film-level structure–property relationships, rather than the performance of viscose textile laminates. Accordingly, this study aims to address this gap by developing and systematically evaluating semi-batch-synthesized PVAc/CNC nanocomposite latexes for use in coating applications.

The reported experimental work focused on the development of a scalable method for incorporating CNCs into PVAc latex via semi-batch emulsion polymerization while maintaining a TSC of 50% to ensure relevance to industrial manufacturing conditions. In water-based emulsion polymerization, semi-batch processes can lead to better efficiency and moderate surfactant use over batch processes. Batch processes can be less efficient in terms of energy and time compared to continuous processes [25]. For intermediate production rate with control over properties, semi-batch process is promising in moderate investment in equipment and flexibility for production of different products [26]. This will bridge the gap between academic research and industrial applications. The research was designed based on findings reported in previous studies [17, 27–29]. To prioritize safety, we adopted a polymerization method that featured the gradual addition of the monomer, initiator, and other components into the reactor. This approach ensures better control over the concentration of the ingredients during the process, facilitating uniform nanocomposite production and achieving a high solid content. This is essential for minimizing transportation costs and the number of processing steps required. The obtained CNC-PVAc nanocomposite latexes were further characterized in terms of bulk wettability, WVTR, FTIR, SEM, polarized microscopy, thermal analysis, and tensile testing.

2 | Materials and Methods

2.1 | Materials

Commercial samples of CNCs featuring sulfate half-ester surface groups (derived from northern bleached softwood kraft pulp) with Na^+ counterions were procured from CelluForce Inc. (Montreal, Québec, Canada). These samples were obtained in a spray-dried form, exhibiting a sulfur content of 0.89 wt.%, equivalent to 0.0462 OSO_3^- per anhydro glucose unit, and an aspect ratio of 20 as reported by the supplier.

To reproduce an industrial process, vinyl acetate (≥99%, Sigma Aldrich) was used without eliminating hydroquinone (contains 3–20 ppm). Ammonium peroxydisulfate $(NH_4)_2 S_2 O_8$ (Alfa Aesar, Kandel, Germany), and sodium bicarbonate (Sigma Aldrich) were used as received. The nonionic emulsifier used was Emulsogen LCN217 (HLB = 17), a fatty alcohol ethoxylated with 21 moles of ethylene oxide from Clariant International Ltd., Muttenz, Switzerland. Partially saponified polyvinyl alcohol (PVOH 8-88), featuring a degree of hydrolysis ranging from 86.7 to 88.7 and molecular weight in the range of 85,000–90,000 g/mol with an approximate degree of blockiness of 50%, was sourced from Kuraray Europe GmbH, Germany, and was employed as received. Distilled water was prepared using Milli-Q (IQ 7000, 18.2 mΩ. cm @25°C).

2.2 | Emulsion Polymerization

The emulsion polymerization of VA in the presence of cellulose nanocrystals was carried out based on the formulations outlined

in Table 1, following the method described by Pakdel et al. [30];, with some modifications. A homopolymer composed solely of VA was synthesized for comparison.

In this study, particular attention was given to identifying and controlling the processing conditions to enable the scaling up of the process. Water was the preferred medium for the process due to the high stability of aqueous cellulose nanocrystal dispersions and potential for achieving a high level of filler dispersion [12]. Polymerization in aqueous media minimizes the use of volatile organic compounds (VOCs) and hazardous emissions. The process sustainability is further enhanced by using renewable, bio-based materials [31]. Achieving a 50 wt.% TSC in the laboratory formulation is essential to meet industrial requirements. The high solid content of nanocomposite latexes simplifies storage, transportation, downstream handling, and reduces energy consumption. For scale-up, formulations developed at the laboratory scale are typically transferred to pilot-scale reactors, which provide precise control over parameters such as the feed rate, temperature, loading, discharge, and safety. Pilot trials are used to validate the process before industrial manufacturing, where latex reactors are commonly designed at capacities of ~10 metric tons with advanced utilities and automation systems.

Polymerization was carried out in a five-neck jacketed glass reactor with a two-liter capacity, equipped with a vertical condenser. The mixture was stirred with a top-head two-story pitched blade Teflon stirrer operating at 140 RPM to achieve homogeneous mixing. A water bath (model Grant, GD120) was used to control the temperature during polymerization. A digital thermometer (PT100 four-wire) was inserted as part of the closure valve at the bottom of the reactor. The reactor was heated by circulating water around the jacket using a water bath pump, reaching a temperature of 70°C. All vapors inside the reactor were guided to the condenser owing to the appropriate sealing around the stirrer and other nozzles (Figure 1).

TABLE 1 | Nanocomposite (NC) formulations made by emulsion polymerization of VA in the presence of CNC through a semi-batch process (amounts in gr).

	Composition [g]					
Component	**PVAc reference**	**NC1**	**NC2**	**NC3**	**NC4**	**NC5**
Distilled water	498.2	498.2	498.2	498.2	498.2	498.2
VA	465	465	465	465	465	465
Ammonium peroxydisulfate	0.78	0.78	0.78	0.78	0.78	0.78
Sodium bicarbonate	0.74	0.74	0.74	0.74	0.74	0.74
Polyvinyl alcohol 8-88	12.78	12.78	12.78	12.78	12.78	12.78
CNC	0	3	6	9	12	15
Emulsogen LCN217	0	3.48	3.48	3.48	3.48	3.48

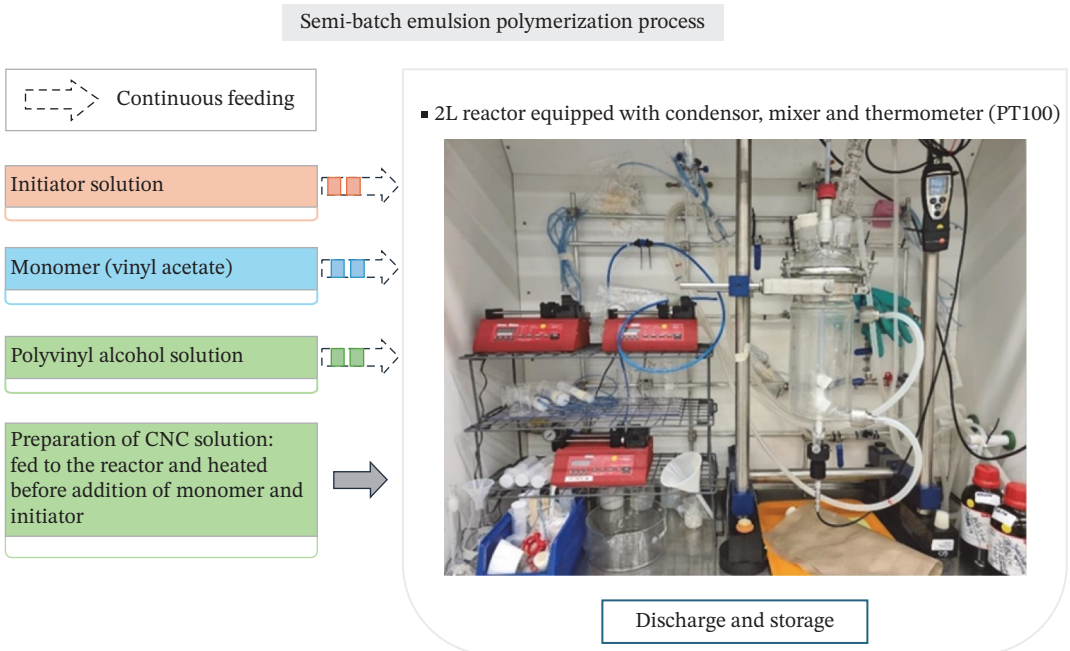

FIGURE 1 | Polymerization set-up.

Before starting the reaction, the CNCs were dispersed in approximately three-quarters of the total water volume in a beaker using a magnetic stirrer for a duration of 3 h. The dispersion was then sonicated in an iced bath for 15 min at 80% amplitude (S24d7 prob, Up400St, Hielscher). Moreover, to ensure efficient dispersion and prevent the aggregation of CNCs during polymerization, 0.6 wt.% surfactant (Emulsogen LCN217) based on the amount of monomer was added to the aqueous CNC dispersion. Subsequently, the mixture underwent a final 3 min of sonication.

The initiator solution was prepared by dissolving (0.69 g) ammonium peroxydisulfate and (0.74 g) sodium bicarbonate in 37.2 g of water. The mixture was stirred with a magnetic stirrer in a beaker for 5 min to ensure complete dissolution.

To prepare the polyvinyl alcohol (PVA) solution, PVA was mixed separately with one-quarter of the total water volume at 23°C using magnetic stirring over a 3 h period without additional heating. To ensure the formation of a stable emulsion at the onset of polymerization, 10 wt.% of the PVA solution was mixed with the CNC dispersion by magnetic mixing for 5 min.

To initiate polymerization, the prepared PVA-CNC solution was poured into the reactor and heated to 70°C. 5 min prior to the addition of the initiator solution, nitrogen gas flow from one of the top nozzles was inserted into the reactor and discharged from the top nozzle of the condenser to eliminate oxygen. Subsequently, 41.3 wt. % of the initiator solution was added over a 2 min period to the reactor, after that the solution was stirred for an additional 5 min at 70°C. Following this, 3 wt.% of VA monomer was introduced to the reactor for 2 min, and then additionally stirred for another 15 min. After stirring for 15 min, the remaining VA monomer, initiator solution, and polyvinyl alcohol solution were added to the reactor using syringe pumps. The addition of VA and initiator solutions was completed within five and half hours, whereas the polyvinyl alcohol solution was completed 1 h earlier.

After the addition of all streams, ammonium peroxydisulfate (0.09 g) dissolved in (15 ml) of distilled water was gradually added to the reactor over a 5 min period to terminate the reaction. Mixing continued for an additional one and half hours to eliminate any traces of active radicals.

The solid content of the obtained dispersions was determined by weighing three samples of each formulation before and after overnight drying in an oven at 105°C. Subsequently, the average values were calculated and reported. All polymerizations were conducted at ~49–51 wt.% TSC.

2.3 | Film Formation

The obtained latex dispersions were converted into films using a film applicator (model ZEHNTNER, ZUA 2000). The latex was poured onto Teflon paper, and a film applicator was used to create a uniform wet film of consistent thickness on the Teflon surface. The thickness of the dry film was measured using an electronic digital gauge meter (Mitutoyo, Elastocon AB, type EV 01F). The obtained films were dried either under laboratory conditions (23°C and 38% relative humidity) or in a climate chamber. All films were uniformly formed without observable defects, and surface skinning was not observed. Films without visible air bubbles were selected for subsequent characterization and testing.

2.4 | Drying Rate of the Films

The drying rate of the films was determined as the percentage of moisture loss per gram of the films per unit of time at 23°C and 38% relative humidity. Wet films of 100 μm thickness were applied on Teflon paper and instantly placed on a four-digit balance. Changes in weight were monitored until equilibrium was reached, and the time was recorded. All data were normalized according to the film unit weight. The differences in TSC were applied to the drying time per unit weight of all samples. The drying rate was calculated as the percentage of moisture loss per gram of film per unit of time.

2.5 | WVTR

The WVTR was assessed at 38°C/90% RH according to ASTM standard E96/E96 M-05. The films were placed on the top edges of a Petri dish filled with a desiccant. Circular films were first cut with a laser-cutting machine from uniform-thickness films, prepared as described earlier, to prevent microcracks within the samples. The covered Petri dishes were placed in a humidity chamber (Memmert HPP108). The moisture absorbed by the desiccant was monitored by periodically weighing the dishes throughout the testing period. Three replicate samples were used for each test. A blank specimen (without desiccant in the Petri dish) was used for each sample group to eliminate the effect of water adsorption by the film.

The WVTR was calculated from the average of three parallel measurements and is expressed as $gh^{-1}m^{-2}$. The WVTR was obtained from the slope of the mass variation (G/t) over time and calculated using Equation (1):

$$\mathrm{WVTR} = \frac{G}{t \times A} = \frac{\left(\frac{G}{t}\right)}{A} \tag{1}$$

Here, G is the steady-state weight gain (g), t is the time (h) during which G occurred, and A is the dish mouth area (m^2). WVTR is reported as $gh^{-1}m^{-2}$. The coefficient of determination (R^2) was used to evaluate the degree of linear correlation between time and the weight gain. An R^2 value close to 1 indicates a strong linear correlation, confirming the presence of a steady-state region appropriate for the WVTR calculation. Permeance was calculated using Equation (2):

$$\mathrm{Permeance} = \frac{\mathrm{WVTR}}{\Delta p} = \frac{\mathrm{WVTR}}{S.(R_1 - R_2)} \tag{2}$$

Here, Δp is the vapor pressure difference, S is the saturation vapor pressure at the test temperature, R_1 is the relative humidity at the water source (expressed as a fraction), and R_2 is the relative humidity at the vapor sink (expressed as a fraction).

2.6 | Polarization Microscopy

A polarized microscope (Nikon LV100ND) equipped with a Nikon DS-Fi3 camera was used to inspect the surfaces of the films. Pristine PVAc and nanocomposite films were formed on

glass slides (100 μm wet film) at a temperature below the T_g of the samples (23°C and 38% relative humidity). All films were investigated at a maximum magnification of 500. Dark-field light of the microscope was applied to explore the surface structure, and bright-field light was used to observe particles with both transmitted and reflected light. All images were collected and analyzed using NIS-Elements 5.41.01 software. The resulting images and 3D topographic pictures were used to describe the surface characteristics of the PVAc and nanocomposite films. The films were also investigated using a Linkam hot-stage heating device connected to a polarized light microscope to study the film formation at elevated temperatures.

2.7 | Scanning Electron Microscopy

Freeze-dried latex dispersions were characterized by scanning electron microscopy (SEM) using a Zeiss Supra 40 VP SEM with a secondary electron detector (SED) at an acceleration rate of 15 kV.3. Subsequently, the samples were coated with a gold layer.

2.8 | Bulk Wettability

The bulk wettability or swelling percentage was determined by immersing three pieces of each film sample (2 cm × 2 cm) in deionized water in a Petri dish for 1 h. Weight gain was monitored, and the results were reported as the average of three samples. The absorbed water or swelling percentage was calculated using Equation (3):

$$(S\%) = (W_S - W_D)/W_D \times 100 \quad (3)$$

W_S and W_D are the swollen and dry weights of the films (PVAc and nanocomposites), respectively.

2.9 | Fourier Transform Infrared Spectroscopy (FTIR)

The approximate peak intensities of the hydroxyl groups in the CNCs and PVAc were analyzed using an ATR-FTIR spectrophotometer (Nicolet iS10, Thermo Scientific, Waltham, Massachusetts, US). The spectra were collected in absorbance mode over a wavenumber range of 400–4000 cm^{-1}. The resolution was 4 cm^{-1} through the accumulation of 64 scans for all the spectra.

2.10 | Thermogravimetric Analysis (TGA)

Thermogravimetric analysis was performed using a TA Instruments Q500 system. Samples weighing ~11–13 mg (dried under laboratory conditions (23°C and 38% RH)) were placed in open platinum pans and heated from 35 to 600°C at 10 °Cmin^{-1} under nitrogen flow of 60 $mlmin^{-1}$. The temperatures corresponding to the 5 wt.% and 50 wt.% mass loss were recorded as T_5 and T_{50}, respectively. The maximum mass loss temperature (T_d) is related to the highest peak value in the derivative thermogravimetry (DTG) curve. The quantity of residue at 600°C was also determined. The weight loss curve and derivative thermograms versus temperature were acquired from the instrument and processed using the TA Universal Analysis 2000 software.

2.11 | Differential Scanning Calorimetry Analysis (DSC)

Differential scanning calorimetry (DSC) was performed using a Q2000 DSC (TA Instruments). The analysis covered a temperature range from −25 to + 220°C, with heating and cooling rates set at 10°Cmin^{-1} under a nitrogen flow of 50 $mlmin^{-1}$. Two heating cycles and one cooling cycle were conducted, and the glass transition temperature was calculated using the data obtained from the second heating run using the midpoint method.

2.12 | Tensile Testing

Tensile testing was performed following the ISO 527–2 standard test method using a Tinius Olsen H10KT Ltd. Universal test machine. The specimens were stretched at a strain rate of 2 $mm.min^{-1}$, and the stress (σ) – strain (ε) relationship was determined until the specimens fractured. The thickness of the specimens was measured using an electronic digital gauge meter (Mitutoyo, Elastocon AB) by taking the average of three measurements. The initial clamping length was set to 25 mm. The load range applied was 5 kN, and the reported results represent the average of five replicates.

3 | Results and Discussion

Polymerizing VA monomers in the presence of CNCs poses several challenges, largely due to the colloidal behavior and interactions of CNCs in aqueous environments. In this study, coagulum formation was observed in three main forms: during polymerization, as deposits on the internal surfaces of the reactor, and by post-polymerization during storage, which is consistent with previously reported research [32]. Our experimental results showed that the presence of CNCs caused latex coagulation. Additionally, the added CNCs induced thixotropic behavior in the solution, which hindered achieving homogeneous mixing.

The surface chemistry of the cellulose nanoparticles is primarily influenced by the extraction procedure [33]. The stability and lower thixotropic effect of the CNCs extracted via sulfuric acid hydrolysis were the reasons for selecting them [34]. This extraction method provides stable aqueous suspensions concurrently with adding a negative surface charge to the CNC [33]. The stability is associated with the electrostatic repulsion of negatively charged sulfate ester groups on the CNCs surfaces [35, 36]. The advantage of sulfuric acid hydrolysis is the creation of a much higher surface charge density, which is an important parameter for surface structure and reactivity of nanocrystals [37–39].

Previous research by Fritz and Olivera [40] observed limited attachment between CNC and polymer particles during nucleation and growth. Therefore, promoting interactions between CNCs and polymer particles is crucial. This can be accomplished by employing protective colloid polymers (or polymeric steric stabilizers), such as polyvinyl alcohol, to form non-covalent bonds or by establishing covalent bonds with the assistance of initiators. Polyvinyl alcohol has been highlighted in numerous papers as an important polymer capable of establishing hydrogen bonding interactions with CNCs [41–43]. Moreover, partially hydrolyzed PVA (around 88% hydrolyzed degree) is commonly

used in synthesis of emulsion polymers [44]. Therefore, the application of polyvinyl alcohol in the synthesis of colloidal nanocomposites could have a stabilizing effect on latex and its interaction with CNCs. Moreover, use of polyvinyl alcohol as a protective colloid shows good mechanical properties of the film [44, 45] and facilitates the stability of particles in emulsions [46]. However, addition of PVA to the polymerization could decrease the water resistance of final film due to the availability of hydroxyl groups [46].

In this study, the percentage of added PVA was reduced from the typical amount used in the adhesive industry (2–5 wt.%) to 1.2 wt.% [46]. The reduction was carried out through controlling the amount of coagulum after decreasing the PVA concentration [47]. This will reduce the effect of PVA on water absorbance and prevent an increase in the concentration of water-soluble molecules in the final film.

To obtain a stable nanocomposite latex, different PVA concentrations were evaluated. Higher PVA content reduced water resistance, whereas lower PVA concentration caused CNC agglomeration and phase separation. Based on the results, the selected amount of PVA, as shown in Table 1, provided PVAc and nanocomposites with stability for more than 8 months.

After polymerization with the assistance of PVA, the TSC was estimated to be between 49 and 51 wt.% for all synthesizes. The addition of CNCs did not interfere with the polymerization of VA, as evidenced by the close agreement between the measured and theoretical TSC values of the synthesized samples.

The use of ammonium persulfate for grafting onto CNCs without prior surface modification has been previously reported by other researchers, including acrylic acid, polyacrylamide, and N, N-(dimethylamine) ethyl methacrylate. Ammonium persulfate offers the advantage of performing grafting without any treatment on the surface of CNCs [48, 49]. In our study, ammonium persulfate was primarily added to an aqueous solution of cellulose nanocrystals at 70°C.

3.1 | Film Formation and Drying Rate

The drying rate, which was determined from the wet films of PVAc and the nanocomposites, is illustrated in Figure 2. The drying rate exhibited a non-monotonic trend with increasing CNC content, whereas all the nanocomposite films dried at a lower rate than the reference PVAc film.

The highest reduction compared to the pristine PVAc film was for NC1, followed by NC4, with reductions of 55.8% and 53.2%, respectively. The drying rate reductions for NC5 and NC2 were lower at 39.1% and 47.1%, respectively. Notably, NC3 exhibited the lowest reduction in the drying rate (10.7%) compared to the reference (PVAc), which may be attributed to the strong interactions between the CNCs and polymer chains. The distinct drying behavior observed for NC3 suggests a complex interplay between the state of the CNCs (free or networked), film morphology, and dynamics of film formation.

The film formation mechanism can be described according to the arrangement of the latex and CNC particles and the loss of water. Steric and electrostatic forces between the particles (latex and CNCs) must be overcome to fabricate a homogenous film. Initially, water was eliminated from the film through surface evaporation, rather than by adsorption into the substrate. The latex particles are arranged in an order based on the secondary forces (intermolecular physical forces) present during the film formation process, while most of the forces in the coalescence are exerted during the evaporation of water [50]. The final film formation is due to the deformation of the latex particles. For interdiffusion of the particles, the film formation process must occur at temperatures above the glass transition temperature (T_g) [51]. In our study, all films were prepared at 23°C, which was below the T_g and above the minimum film-forming temperature (MFFT).

In terms of appearance, the pristine PVAc film was transparent, whereas the nanocomposite films appeared hazy due to the increased dosage of CNCs. The reason for this haziness might be related to formation of air voids or holes in the film due to the

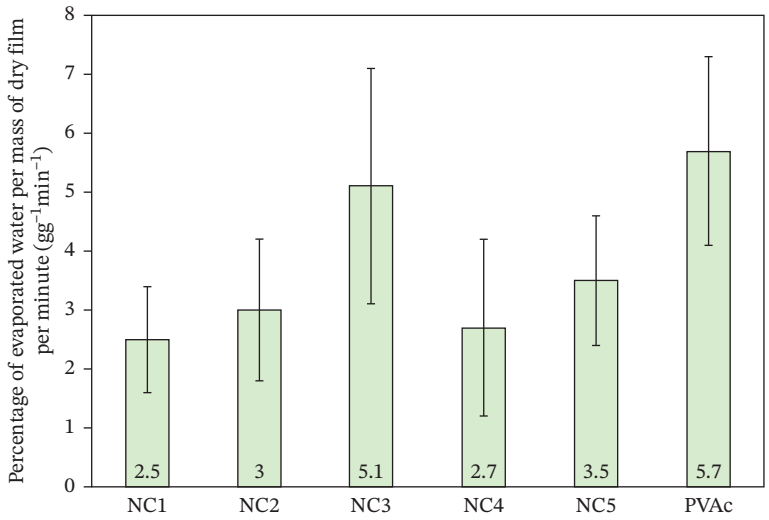

FIGURE 2 | Drying rate of the PVAc and nanocomposite (NC1 to NC5) films, percentage of evaporated water mass per mass of dry film per minute (g.g^{-1}min^{-1}).

incomplete particle deformation and coalescence [51]. The micrographs obtained by polarization microscopy indicated that these structures in the films could be a reason for light scattering. A faster evaporation rate could create structures with less order [51]. This effect was investigated using a Linkam hot-stage apparatus under continuous microscopic observation. However, no interdiffusion of polymer particles was observed up to 70°C.

The incorporation of surfactants or protective colloids in film formation is a known phenomenon often linked to the rate of water evaporation. While for some cases these additives decrease the evaporation rate, it is possible also to increase the evaporation rate [51]. Surfactants can plasticize latex, and the longer ethylene oxide (EO) chains in surfactants cause higher water adsorption and less integration of the film. The application of nonionic surfactants in nanocomposites may be considered as one of the reasons for the lower drying rate of nanocomposites compared to the PVAc reference.

The presence of CNCs in the PVAc films hindered water evaporation, resulting in a slower drying rate compared to PVAc. This could be due to the formation of hydrogen bonds between the CNCs and water molecules, which may hinder water evaporation. It has been reported that the repulsive electrostatic force could offset the nanocomposites coalescence stage of film formation [51]. The repulsive forces between the CNCs may influence the drying rate of the nanocomposites. A reduction in the number of unconnected CNCs likely minimized their disruptive effect on capillary forces during film drying [51]. In our study, negatively charged CNCs acted as an opposing force during film formation.

3.2 | WVTR

Figure 3a illustrates the WVTR of the nanocomposite films (NC1-NC5) in comparison to the PVAc reference, determined at 38°C and 90% relative humidity. The calculated WVTR values indicated that the incorporation of CNCs at moderate loadings decreased WVTR in the nanocomposite films compared to the PVAc reference (19 $gh^{-1}m^{-2}$). NC1 and NC2 exhibited nearly identical WVTR of 13 $gh^{-1}m^{-2}$. Further increasing the CNC content for NC3 resulted in a further slight reduction to 12.8 $gh^{-1}m^{-2}$. However, at higher CNC loadings, NC4 showed an increase in WVTR to 15.2 $gh^{-1}m^{-2}$, although it was still below the PVAc reference value of 19 $gh^{-1}m^{-2}$. At the highest CNC loading (NC5), WVTR exceeded the reference film, likely due to CNC agglomeration and incomplete integration into the matrix. The presence of excess hydroxyl groups, confirmed by FTIR, suggests unbound CNCs that increase water affinity. In addition, swelling effects at high CNC concentrations may have generated microchannels that facilitated vapor transport.

Notably, NC3, which exhibited the lowest reduction in drying rate, as discussed in the drying rate section, also demonstrated the lowest WVTR. This behavior might be related to the optimal CNC distribution through various possible bonds, which facilitated efficient drying while enhancing the barrier properties. The effective integration of CNCs was also confirmed in the swelling test of the nanocomposites, where only nanocomposites with moderate CNC loading remained stable after the test.

The calculated permeance is shown in Figure 3b. The effect of the CNCs on permeance was different from that reported by Nozaki and Lona [23]. They reported in their experiment that the incorporation of CNCs via mixing or in situ polymerization did not differ, and in both cases, the nanocomposites showed higher permeance than the PVAc reference. In our study, the performance evaluation showed that, except for NC5, all nanocomposite films had lower permeance than the reference.

3.3 | Polarization Microscopy

The images obtained from the polarization microscopy studies are shown in Figure 4. For films containing CNC, a higher CNC loading promoted the formation of mosaic patterns. The surface of the pristine PVAc film appeared similar to that of NC1, displaying closely packed particles and a smoother morphology. For pristine PVAc, the polymer film exhibited streak-like entanglements, and the mosaic pattern structure was not visible.

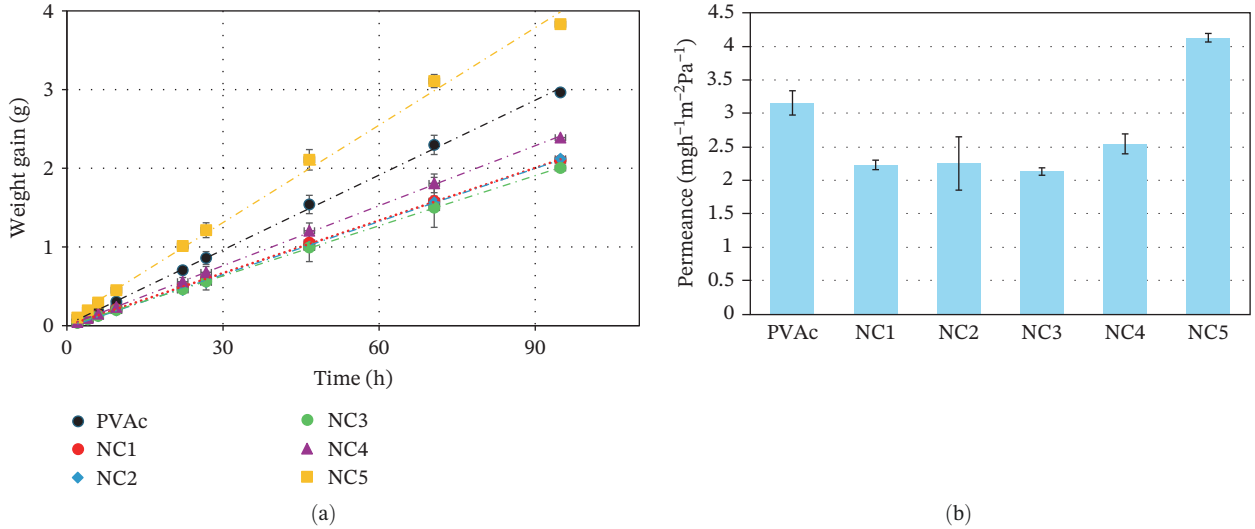

FIGURE 3 | (a) Water vapor transmission rate for PVAc and nanocomposite at 38°C and 90% relative humidity, (b) Permeance of the samples.

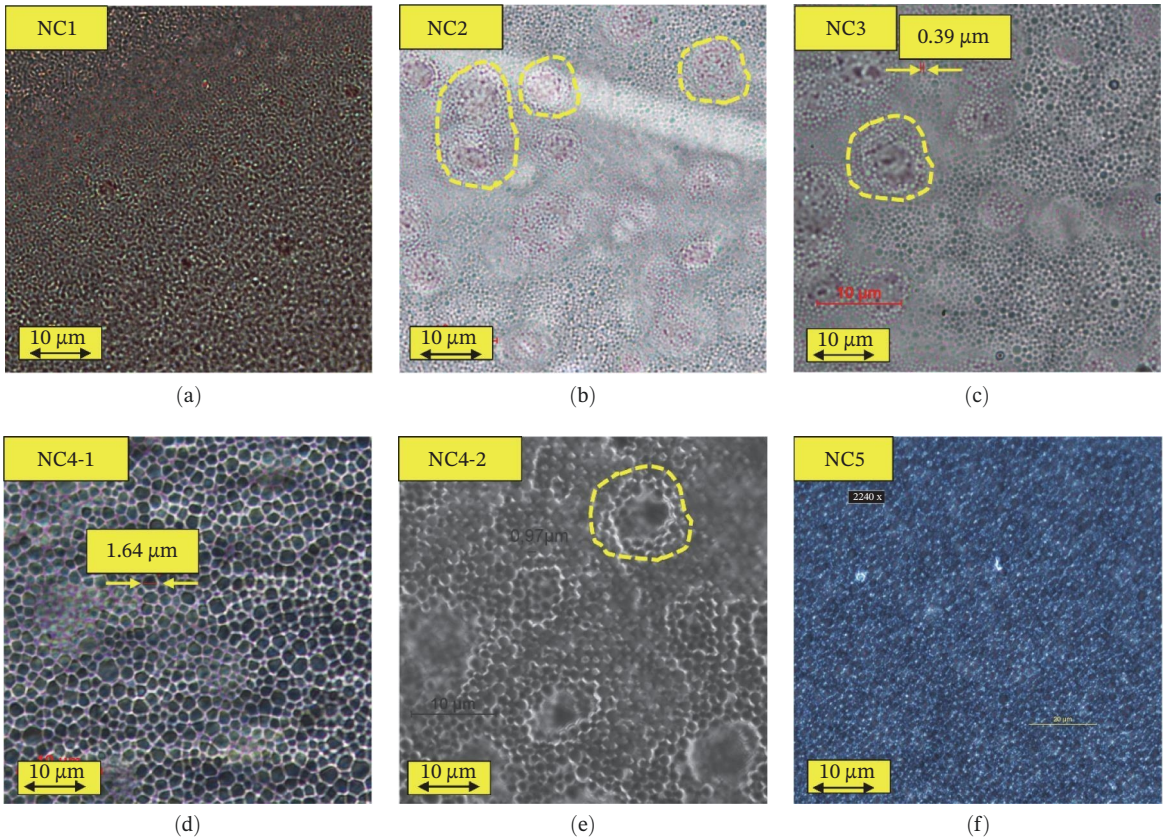

FIGURE 4 | Images of the surface of the nanocomposite films dried on glass slides in laboratory (100 µm wet film), (a) NC1, view in dark field light, (b) NC2, view in dark field light with highlighted sections showed same pattern but in different level, (c) NC3, view in dark field light with highlighted section showed same pattern but in different level, (d) NC4-1, view in dark field light, (e) NC4-2, view in bright field light with highlighted section showed same pattern in different level, (f) NC5, view in dark field light.

The cellulose nanocrystals caused an uneven film surface, and mosaic patterns of different sizes were created. The size of the mosaic pattern increased with increasing CNC dosage. The maximum size of the mosaic pattern was ~1.64 µm for the films NC4 and NC5. NC5 had a structure similar to that of NC4 under dark-field microscopy; however, there was no clear indication of polymer particles under bright-field light. For NC4 (Figure 4e), individual polymer particles with an average diameter of ~0.97 µm can be distinguished, indicating the absence of interdiffusion. This result may explain the WVTR observed for NC4, as the limited interdiffusion likely led to a film structure with more-open pores. Although deformation of latex particles facilitates closer packing and smoother surface, it is not always a prerequisite for film formation [51]. Deformation will occur by overcoming the capillary and interfacial forces over the rigidity of latex particles [52]. As long as particles keep their original spherical shape, the van der Waals forces seem to be weaker than the capillary forces [52]. Incorporation of polyvinyl alcohol in all film samples could also act as a barrier against the coalescence of the polymer particles because of the surface hydrolysis caused by polyvinyl alcohol [53].

When the polymer particles were detected, they were nearly identical in size and homogeneous in shape without deformations. Film formation under T_g could be the reason for the particles remaining intact. To confirm the results, the film formation of NC4 was carried out at 70°C, which is above the T_g. A micrograph of the surface shows intact particles (Figure 4e) even when the film was annealed at 70°C. The interdiffusion of the particles can only be achieved when the nanocomposite film is heated to 150°C. This was observed when the nanocomposite films were subjected to heating on the Linkam hot stage while being monitored under the microscope. Therefore, the reason for the particles remaining intact might be the repulsive forces between the particles in the nanocomposites. The presence of CNCs may impede the diffusion of polymer particles similarly to hydrophilic layers or shells of latex particles [51]. Under the microscope, the samples showed a homogeneous surface without any detectable aggregation. Specific areas indicated by the yellow round shapes in Figure 4 are related to the unevenness of the film's surface.

The surface roughness of the films was examined using optical microscopy, as shown in Figure 5. The surface of the PVAc film was completely smooth without any topographic pattern; therefore, it is not shown in Figure 5. The surface roughness of the film was correlated with the concentration of incorporated CNC. As the CNC loading increased, the surface roughness of the film increased.

Incorporating higher concentration of protective colloids or surfactants could result in a higher coverage of particles and lead to a smoother surface of the film [54]. In our study, the amount of protective colloid, polyvinyl alcohol (PVA), was kept constant for both PVAc and nanocomposites. During drying, the concentration of surfactants in the residual water between the polymer particles increased, effectively acting as an electrolyte. The

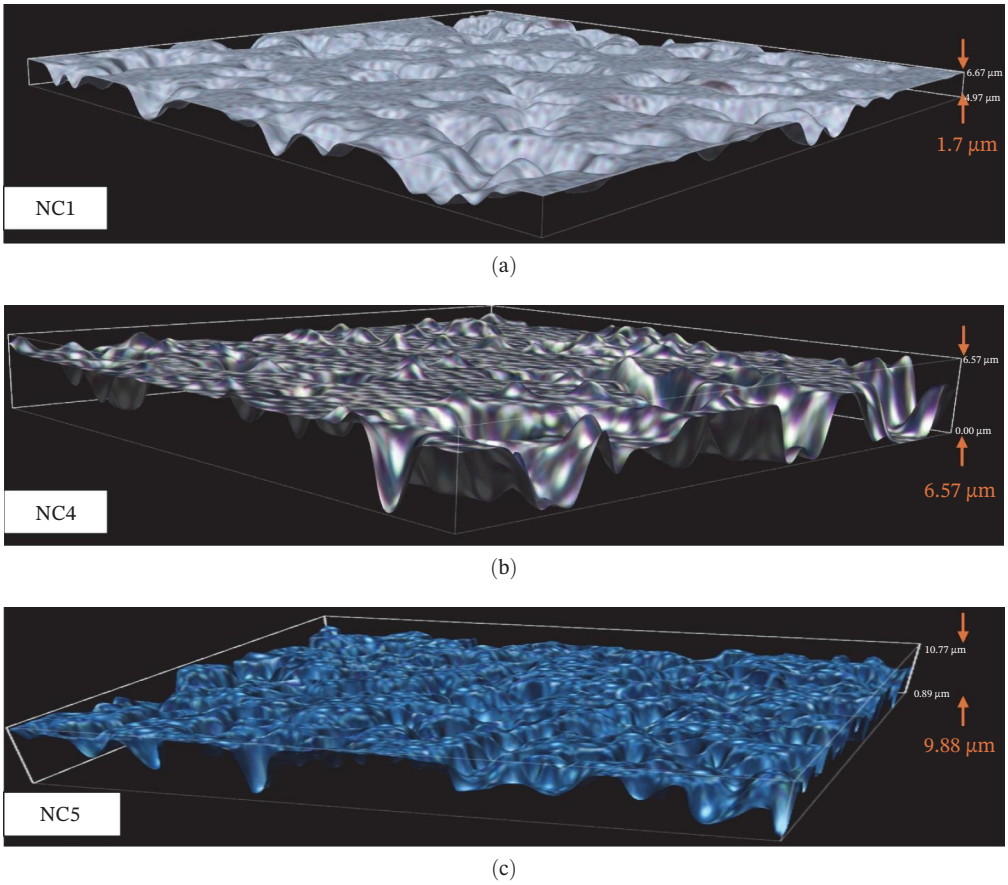

FIGURE 5 | Topographic pictures of nanocomposite films, (a) NC1, (b) NC4 and (c) NC5.

micrographs suggest that the increased electrolyte concentration may have been compensated by the rearrangement of particles into varying topographies, such as peaks and valleys. Therefore, the stronger repulsive forces between the particles may be the reason for the higher roughness. Furthermore, the repulsive interactions of the negatively charged CNCs may have contributed to the surface irregularities in the nanocomposites.

As illustrated in Figure 5, higher CNC loadings increased the roughness of the film surface. Moreover, a higher CNC dosage created a surface with a higher number density of holes in a specific area. The topographic profiles of NC4 and NC5 showed the highest roughness among all the samples. For instance, while the variation between the highest and lowest sections throughout the topography image of the films of NC4 and NC5 could reach ~10 µm, it was only ~1.7 µm for NC1.

3.4 | Scanning Electron Microscopy

Figure 6 shows the morphologies of the freeze-dried PVAc and PVAc-CNC samples. As shown in Figure 6, a higher CNC content in the nanocomposites resulted in an increase in the average particle size (D) and a broader size distribution of the particles. The average particle size of the reference PVAc (a) was 0.7 µm, while an increase was observed for NC3 (b) and NC4 (c), reaching 0.92 µm and 1.8 µm, respectively.

SEM analysis revealed that the increased CNC loading influenced the polymer particle size, potentially affecting the film packing density and porosity. The SEM results support the conclusions from polarization microscopy that the size of the mosaic pattern increased with increasing CNC dosage. Similar results were reported in a study conducted by Geng et al. [22], who demonstrated that increasing the CNC content led to an increase in particle formation. The authors attributed this phenomenon to the poorer miscibility between CNC and PVAc generated by the direct mixing process. The CNCs used in this study were obtained via sulfuric acid hydrolysis. The negatively charged sulfate half-ester groups on their surface dissociate in water, contributing to the formation of ionic species in the dispersion. This increased ionic strength of the medium reduces the electrostatic repulsion between the dispersion particles which promotes aggregation and leads to increased particle size and broader size distribution [55].

3.5 | Bulk Wettability

The swelling tests of the film samples were conducted by immersing the films in deionized water in Petri dishes. First, the films were dried and weighed at 23°C and 38% relative humidity. Subsequently, the films were placed in Petri dishes and covered with deionized water for 1 h. The swollen films were dried using paper tissue to eliminate excess water and weighed immediately. Figure 7 shows the appearance of the films following the swelling test.

As is shown in Table 2, incorporating CNCs by 0.64 wt.% of total monomer (NC1) content caused a reduction in swelling

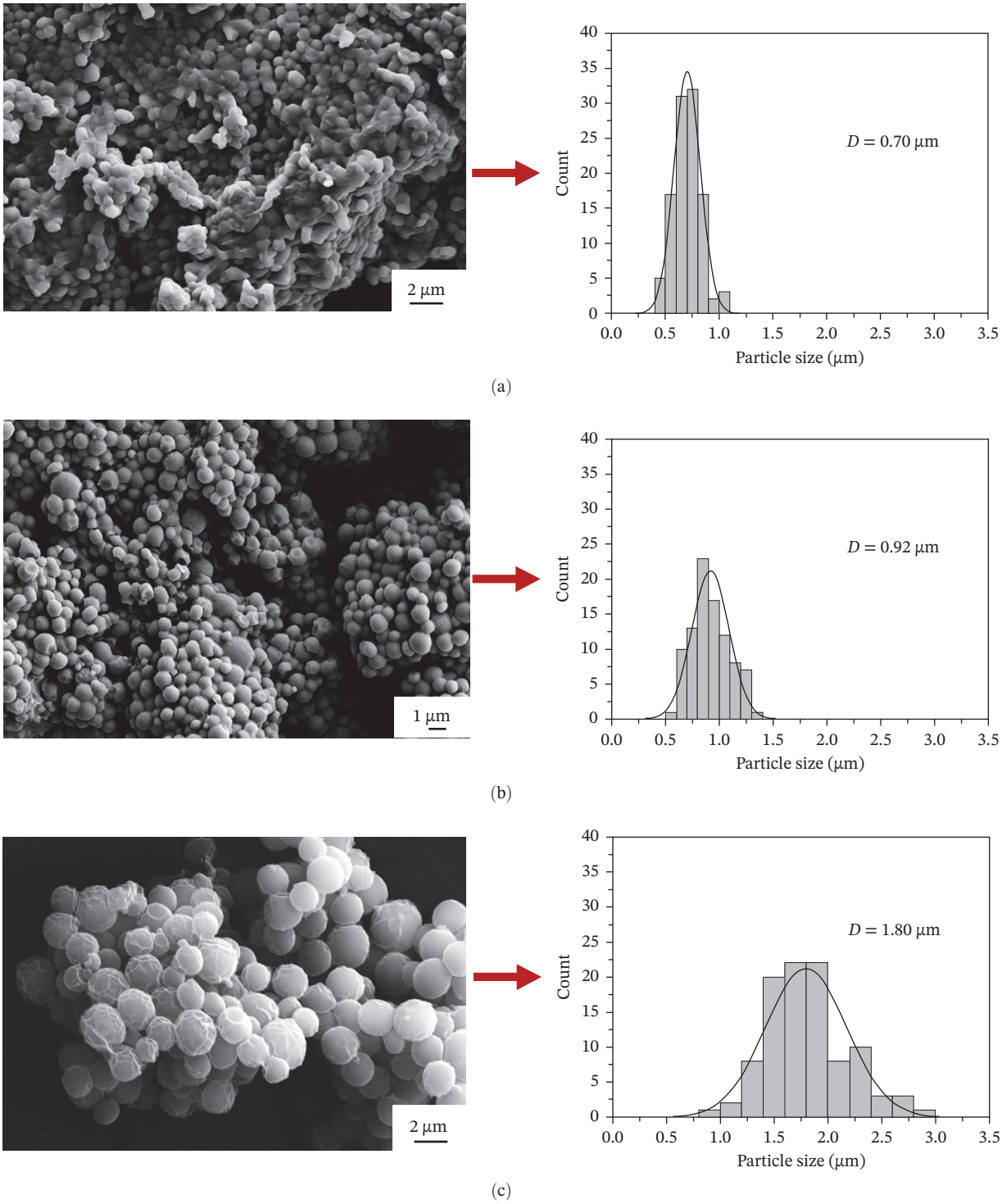

FIGURE 6 | SEM micrographs and particle size distributions for spray dried latex particles (a) PVAc, (b) NC2 and (c) NC4.

percentage to almost half compared to PVAc. The effect of CNCs at a higher loading (1.29 wt. %) and 1.93 wt.%, for NC2 and NC3 respectively, caused the swelling percentage to increase around 2% compared to NC1. The lowest swelling percentage of 14.85 wt. % was for NC4 with 2.58 wt.% CNC dosage. Increasing the CNC dosage to 3.22 wt.% (NC5) caused a sudden increase in swelling percentage to 49.55% which was 9.3% higher than for the pristine PVAc.

The swelling test is an indicative test for the existence of capillary networks in polymer films [51]. By maintaining the same PVA dosage, the observed variation in water absorption can be attributed to the presence and concentration of CNCs. The wettability of CNC particles could increase the particle–particle contact (wetting) and suppress formed voids similar to coalescing aids [51]. This could be attributed to the effect of CNC swelling on decreasing the available pathways within the nanocomposite film. The swelling of CNCs might reduce the free spaces or pores in the nanocomposite film. Another interpretation is the formation of interactions between the polymer chains, protective colloids, and CNC particles. For the pristine homopolymer, PVAc chains and

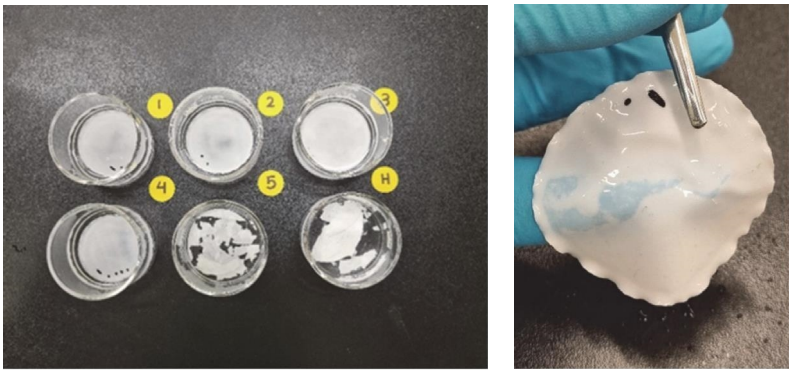

(a) (b)

FIGURE 7 | (a) PVAc (H) and nanocomposite films (NC1 to NC5 illustrated as 1–5) after swelling test. (b) Film appearance of NC1 to NC4 after swelling test.

TABLE 2 | Bulk wettability or swelling percentage of PVAc and nanocomposites.

Samples	Wt. % of CNC based on weight of VA	Dried weight (W_d) [g]	Swelling weight (W_s) [g]	Swelling percent (S%)	Condition of the film after 1 h
PVAc	—	0.60	0.84	40.25	Disintegrated
NC1	0.64	0.29	0.36	20.77	Intact
NC2	1.29	0.27	0.33	22.32	Intact
NC3	1.93	0.29	0.35	22.23	Intact
NC4	2.58	0.28	0.33	14.85	Intact
NC5	3.22	0.22	0.33	49.55	Disintegrated

protective colloids (PVA) were present in the film. PVA can be partially dissolved and remains between the polymer particles. It is also possible for PVA to physically absorb or chemically bond to PVAc polymers [44]. For PVAc, the presence of PVA between PVAc chains leads to increased water absorption, resulting in the disintegration of the film. The characteristics of the nanocomposites could differ owing to the interactions between CNC, PVA, and PVAc. For moderate addition of CNCs (between 0.64 and 2.58 wt.%; Table 1) swelling of the film decreased which could be a result of consumption of available hydroxyl groups, either on the CNC particles or the PVA. For NC1 to NC4, the nanocomposite film remained intact after swelling (Figure 7b), whereas PVAc and NC5 were disintegrated into smaller fragments (Figure 7a). The stabilization of the nanocomposite films (NC1 to NC4) could be related to the secondary bonds between the polymer chains, PVA, and CNCs. These bonds are formed by the consumption of hydroxyl groups, which consequently makes the film more stable and less sensitive to water absorption. For NC5, FTIR analysis revealed the highest number of available hydroxyl groups, which may account for the greater water uptake observed in the swelling test. As the CNC loading was highest in NC5, a large portion of CNCs may have remained dispersed but unbound after synthesis. These unbounded CNCs in NC5 could be the reason for agglomeration into clusters and dispersion of CNCs within water with weak ionic bonds. These ionic bonds can be easily disconnected because of water adsorption. This is also probable for PVAc when PVA molecules are physically dispersed between the polymer chains. They can absorb water in higher amounts of polymer chains and can dissolve in water. This caused the PVAc film to become dimensionally unstable and disintegrated in water.

3.6 | FTIR Spectroscopy

FTIR spectroscopy was used to identify the specific chemical interactions between the functional groups after incorporating the CNCs into the PVAc latex. Figure 8 shows the FTIR spectra of pristine PVAc and nanocomposites with different CNC dosages.

The broad peak between 3200 and 3500 cm^{-1} corresponds to the stretching of the O—H group with intramolecular and intermolecular hydrogen bonds. FTIR analysis indicated variations in the availability of hydroxyl groups, which may influence the interaction of water within the film through hydrogen bonding. The highest intensity of this peak appeared at 3340 cm^{-1} for NC5, followed by PVAc at 3350 cm^{-1}. This broad peak was comparatively weak for the other nanocomposites. (Figure 8b)

As the amount of polyvinyl alcohol was the same in all samples, the disappearance of the broad band between 3200–3500 cm^{-1} indicates the formation of chemical bonds that consume hydroxyl groups. However, for the highest CNC dosage in NC5, this peak appeared with higher intensity, which could be a consequence of the free cellulose nanocrystals dispersed in the water phase. The existence of chemical bonds between the hydroxyl groups was experimentally confirmed in the bulk wettability experiment. During the experiment, the films NC1–NC4 remained intact after swelling in water. The results confirmed

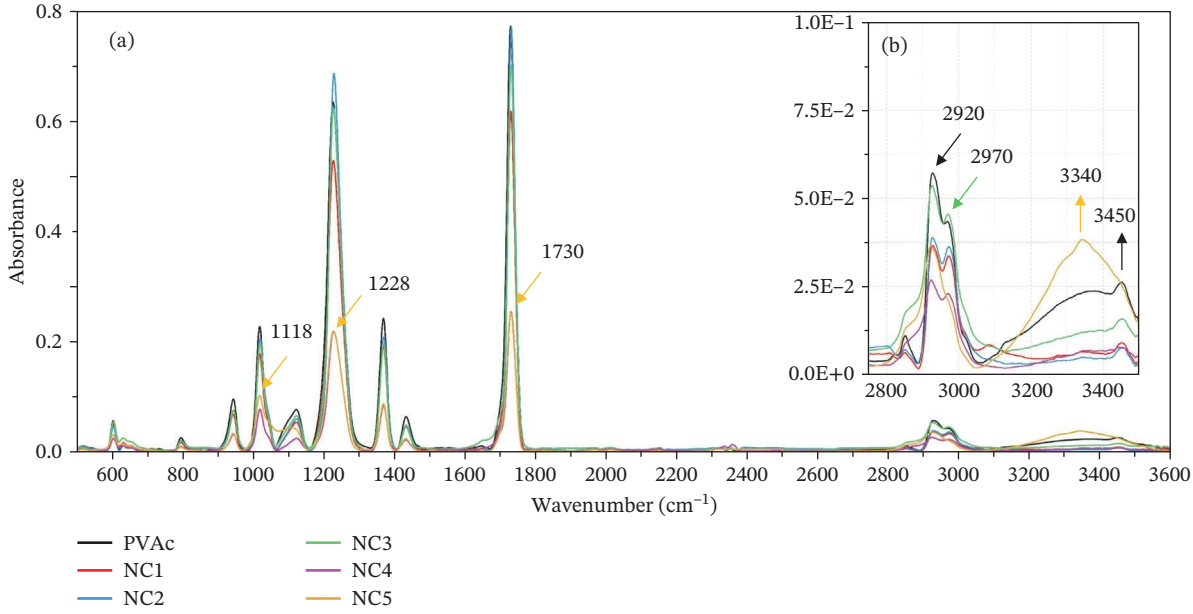

FIGURE 8 | FTIR spectra for PVAc and nanocomposites 1 – 5 (a) with the expanded OH group range to the right (b), Reproduced from [6], under the Creative Commons CC-BY-NC-ND license.

the formation of stable chemical bonds between the CNCs and PVAc. The peaks at 2920 and 2970 cm^{-1} are typical C—H stretching peaks for alkyl groups. Incorporating CNCs in the polymerization process reduces the intensity of these bonds. The highest reduction was observed for NC4. The stretching at 2920 cm^{-1} was the only peak for NC5, and the stretching peak at 2970 cm^{-1} disappeared. The intensity of the carbonyl stretch peak at 1730 cm–1 decreased as the CNC content increased. The highest decrease was observed for NC4 and NC5. The change in intensity of the peak also appears for the stretch at 1228 cm$^{-1,}$ which is characteristic of ester bonds.

3.7 | Thermogravimetric Analysis

Figure 9 shows the TGA results for all samples, which indicate two main degradation steps. The first degradation step occurred between 270 and 370°C, accounting for ~70% of the mass loss, whereas the second degradation step, occurring between 370 and 470°C, contributed ~25% of the total mass loss. The initial elimination of acetic acid and appearance of unsaturation for PVAc is reported to occur at 160°C [56]. The evolution of carbon double bonds in the polymer backbone throughout the first degradation step concurrently with the elimination of acetic acid could be possible reasons for high degradation during the first step [56–58].

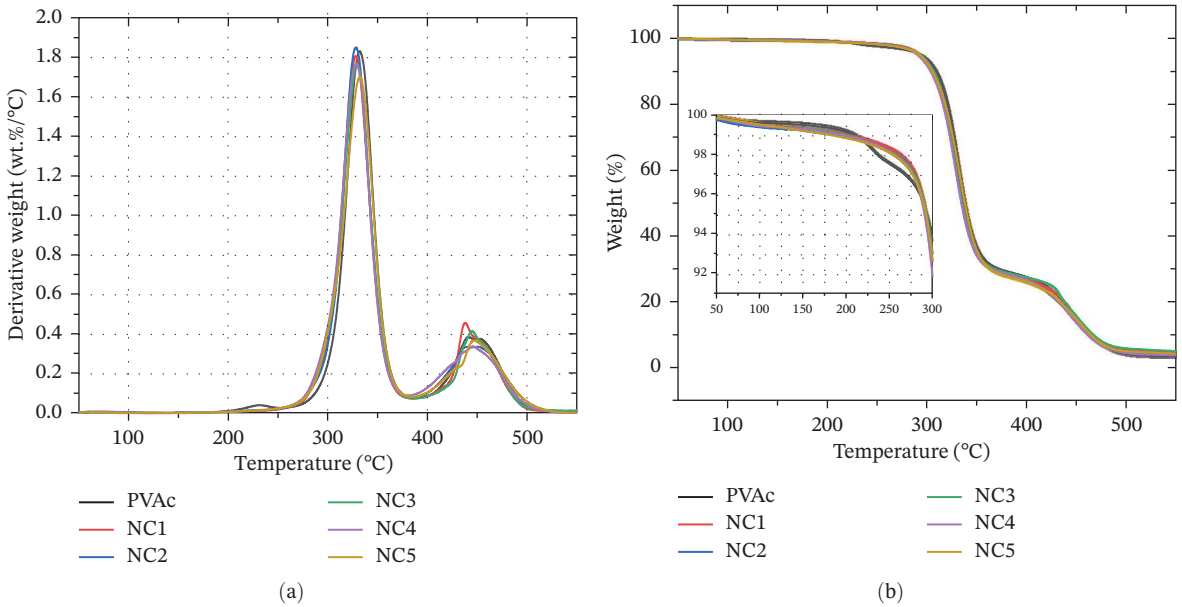

FIGURE 9 | TGA curves of PVAc and nanocomposites (a) Derivative weight changes by the temperature for all samples, (b) Weight loss versus temperature for all samples.

As illustrated in Figure 9b, PVAc underwent initial thermal degradation at ~339°C, followed by lower mass loss during the second step between 441 and 452°C. The synthesized PVAc also showed a 1.6 wt. % mass loss at 232°C, which was not observed for the nanocomposites. The first degradation of PVAc has previously been reported to occur in the range of 150–220°C [59]. In the study conducted by Nozaki and Lona [23], the thermal degradation of a PVAc-CNC nanocomposite was reported at slightly lower temperatures (between 100 and 130°C), whereas in our experiment, it was observed at higher temperatures (T_5 ~290°C). The mass loss at 232°C could not be related to the existing oligomers or free entangled monomers present in PVAc because the same procedure was applied for all polymerizations (PVAc and nanocomposites). Therefore, this could be related to the effect of CNCs on the thermal stability before the onset of the first degradation step. It can be assumed that the CNC blocks water/vapor to hydrolyze the ester. The enhanced stability below 250°C may be attributed to hydrogen bonding and physical interactions between the hydroxyl groups and PVAc chains, which restrict chain mobility and delay segmental motion. The higher stability might be explained by the interactions between the abundant hydroxyl groups available on the CNCs surface and the acetate side groups of PVAc. These interactions could delay the formation of carbonyl groups or restrict the release of acetic acid. The hydrogen bonding interaction between the hydroxyl groups of CNCs and the carbonyl groups was previously identified as the key factor contributing to the enhancement of thermal and mechanical properties in the nanocomposite [60]. The temperature at 5 wt.% mass loss (T_5) was higher for pristine PVAc compared to CNC containing films. The reduction was higher when the CNC loading increased to NC4. This trend was repeated for the temperature at 50 wt.% mass loss (T_{50}) where addition of CNCs caused reduction of temperature at 50% weight loss. The reduction in stability due to the addition of CNC was consistent with a previous study conducted by Girouard et al. [61]. Lower degradation temperatures may be due to the partial decomposition of CNCs and the formation of acidic products that promote chain scission, as previously reported. It has been also mentioned that efficient interfacial adhesion and well dispersed nanocellulose between polymer matrix are required for the improvement of thermal stability. According to Figure 4, the nanocellulose particles are dispersed in the matrix in a way that forms a special pattern, which could be evidence of the non-homogenous dispersion of nanocellulose between polymer particles. CNCs extracted through sulfuric acid hydrolysis typically exhibit limited thermal stability [48]. Higher amounts of sulfate groups contribute to thermal degradation at lower temperatures [36, 62, 63]. In our study, according to the supplier, cellulose nanocrystals were extracted through sulfuric acid hydrolysis, which converts one of every eight primary alcohols on the surface to sulfate half-esters. The results showed a reduction in T_5 and T_{50} due to increased cellulose nanocrystal loading. Cellulose nanocrystals have a large surface area which could increase the exposure area to heat, appearing only when good dispersion was achieved [63]. As a result, increasing the CNCs content could decrease the onset of degradation temperature.

The thermal stability of the reference PVAc and nanocomposites in this study was higher than that in the study conducted by Nozaki and Lona [23]. While all PVAc and nanocomposites in previous studies showed degradation below 200°C, our experiment demonstrated degradation at ~290°C.

3.8 | Differential Scanning Calorimetry (DSC)

The incorporation of CNCs into PVAc caused a slight reduction in T_g; however, the reduction at the maximum dosage (NC5) was lower than that of the other dosages (Figure 10). The reduction of T_g could be a consequence of interrupting the original interaction between the chains which led to a higher microphase separation in the polymer matrix and, consequently, a decrease in T_g [63]. Moreover, incorporation of nonionic surfactant in synthesis of

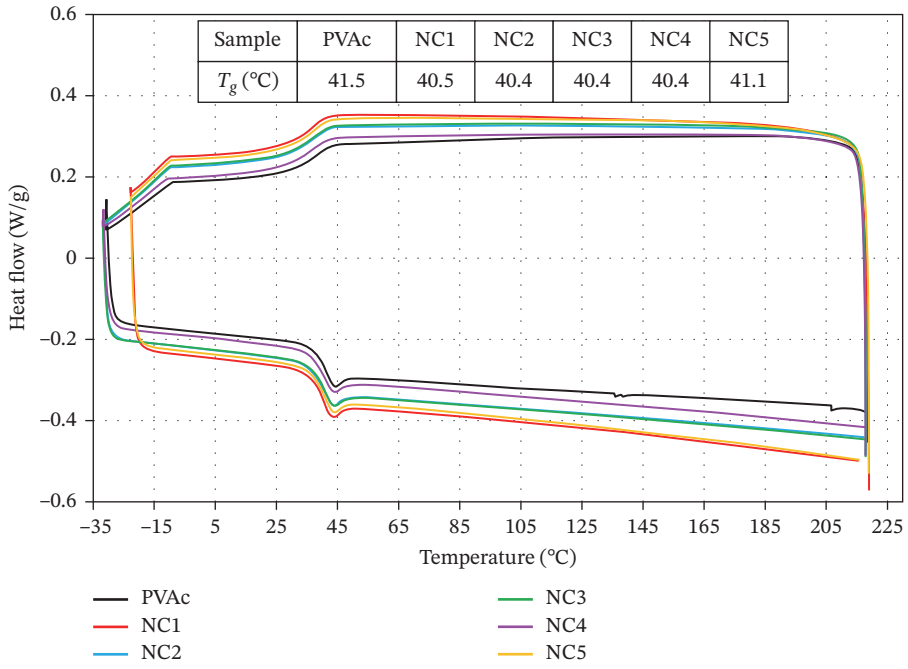

FIGURE 10 | DSC curves for PVAc and nanocomposites.

nanocomposite could influence T_g [64]. The plasticizing effect of the surfactant might be the reason for the reduction in the glass transition temperature of the nanocomposites.

3.9 | Mechanical Properties of PVAc and Nanocomposites

Tensile testing was performed on films formed under two different conditions to determine the effect of the drying conditions on the mechanical properties of the final film. The purpose of this study was to determine whether particle coalescence differed under the two conditions or whether capillary forces induced by evaporation played a dominant role. The measured ultimate strength, elongation at break, yield strength, and modulus are reported in Table 3. Drying was performed at 22°C and 80% relative humidity in a climate chamber and at 23°C and 38% relative humidity (laboratory conditions). The temperature of the humidity chamber was set to one degree lower to prevent the actual temperature from exceeding 23°C owing to possible temperature fluctuations.

Under both drying conditions, pristine PVAc exhibited the highest values for the maximum elongation at break and ultimate strength among all samples, and plastic behavior was not observed in any of the samples. The absence of plastic deformation in the nanocomposite is consistent with the findings of a previous study by Nozaki and Lona [23]. This could be due to the local stress created by poor dispersion or connections and the brittleness of the film [65, 66]. The restricted mobility of the polymer chains can be attributed to the formation of various interfacial bonds between the polymer and CNCs. Microscopic analysis (Figure 4) revealed the development of mosaic patterns on the surface of the nanocomposite film, which became increasingly pronounced with higher CNC loadings. This could indicate a reduction in particle coalescence during film formation. This observation, together with the increase in particle size at higher CNC contents (Figure 6), suggests that the CNCs act as physical barriers to polymer diffusion. SEM analysis presented in Figure 6 shows that the incorporation of CNCs increased polymer particle size, suggesting adsorption of CNCs onto the particle surfaces [66]. For larger polymer particles, CNCs are likely primarily adsorbed onto their surfaces, whereas for smaller particles, CNCs may interact with multiple polymer particles and with other CNCs, forming a network. In our study, the presence of large polymer particles may have hindered network formation or approached the percolation threshold. As shown in Table 3, the measured ultimate strength for all nanocomposite samples shows better results for the films dried under laboratory conditions at lower humidity compared to films dried under humidity chamber conditions. Faster drying of the films under laboratory conditions could create stronger capillary forces, which force the particles to arrange in a closer arrangement, creating stronger films. Although, the capillary forces do not determine the spreading the particles, but it could have an effect on closer packing between the particles [51].

Our results showed that the reduction in the ultimate strength was not directly proportional to the increase in the CNCs content. Except for NC4, increasing the CNCs content increased the ultimate strength. It has been reported that CNCs with high loading increase intermolecular interactions, which may promote aggregation and hinder filler dispersion [67]. The highest ultimate strength was achieved for NC5, which contained the highest loading of CNCs. This could be the reason for the arrangement being closer to the percolation threshold [14]. At higher CNC loadings, the enhancement of the ultimate strength might be due to the network formation by CNC particles. However, this could not be proven by examining FTIR spectra of the samples (Figure 8b). The high level of hydroxy bonds for NC5 also showed a shift to lower bonds, making it difficult to interpret the extent to which CNCs were involved in the chemical bonds with the polymer, while the addition of more CNC increased the number of hydroxyl groups in the sample. For NC5, the hydrogen bonds between CNCs, which were created by higher amounts of CNCs, might be the reason for the higher ultimate strength.

Because our goal was to maintain the TSC of the nanocomposites at ~50 wt.%, increasing the CNC content beyond the level used in NC5 was not feasible under the processing conditions. Consequently, it was difficult to determine the effect of the CNCs on the ultimate strength at higher concentrations.

The lower T_g values of the nanocomposites observed in the DSC analysis may correspond to their reduced ultimate strength. The microstructural separation observed under polarized microscopy (Figure 4) likely disrupted the intermolecular interactions, leading to a non-uniform stress distribution and localized resistance

TABLE 3 | Tensile test for PVAc and nanocomposite films.

	Ultimate strength [MPa]		Elongation at break (%)		Yield strength [MPa]		E modulus [MPa]	
Sample	Drying condition 1[a]	Drying condition 2[b]	Drying condition 1	Drying condition 2	Drying condition 1	Drying condition 2	Drying condition 1	Drying condition 2
PVAc	35.1 ± 2.6	33.6 ± 2.4	1.89 ± 0.2	2.18 ± 0.5	35.1 ± 2.6	33.6 ± 2.4	2230 ± 134	2170 ± 147
NC1	NA	7.71 ± 3.7	NA	1.18 ± 0.4	NA	7.4 ± 4	NA	881 ± 550
NC2	7.3 ± 2.5	10.5 ± 3.7	1.3 ± 0.6	1.6 ± 0.5	7.1 ± 2.7	9.5 ± 2.9	1102 ± 689	1350 ± 313
NC3	15.3 ± 4.5	17.5 ± 5.8	1.4 ± 0.3	1.4 ± 0.2	14.5 ± 6	17.5 ± 5.8	3763 ± 2578	1060 ± 627
NC4	1.9 ± 0.9	9.7 ± 4.7	1.3 ± 0.2	1.2 ± 0.2	1.9 ± 0.9	8.7 ± 5.8	626 ± 38	1380 ± 972
NC5	16.1 ± 2	22.2 ± 2.9	1.3 ± 0.2	1.5 ± 0.1	16.1 ± 2.2	23 ± 3.1	2140 ± 937	2330 ± 1490

Abbreviation: NA, not available.
[a]Drying condition 1: 22°C/80% Relative humidity (climate chamber condition).
[b]Drying condition 2: 23°C/38% Relative humidity (laboratory condition).

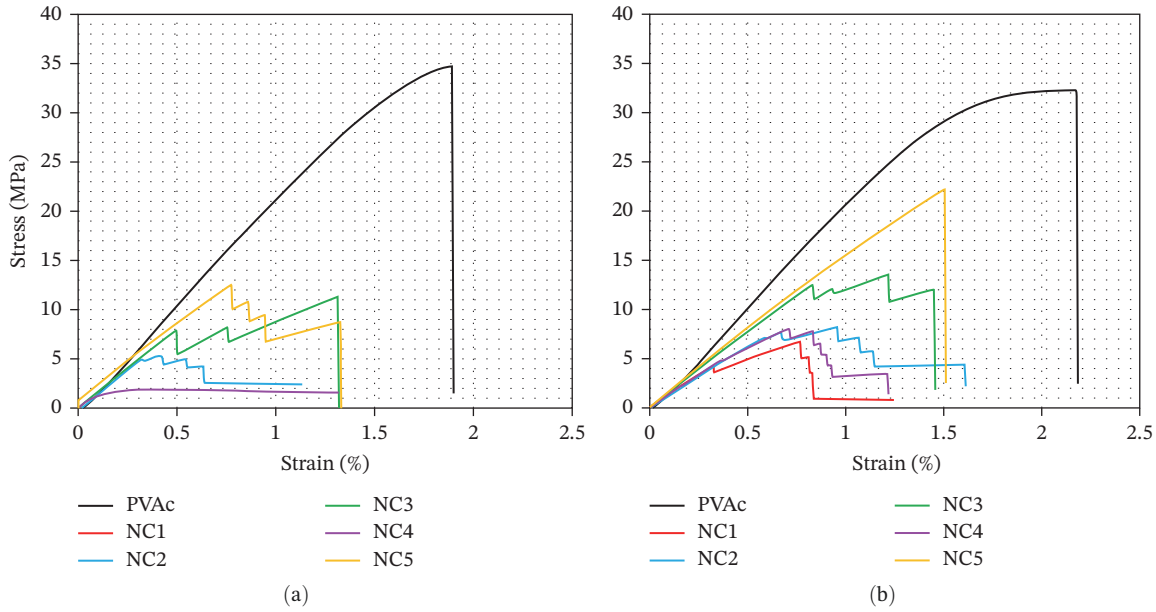

FIGURE 11 | Stress–strain curves of PVAc and nanocomposite films: (a) Samples dried under climate chamber conditions, (b) Samples dried under laboratory conditions.

to fracture. The relatively stable T_g of NC5 suggests improved interfacial interactions and partial CNC network formation, which restricts chain motion and mitigates plastic deformation. The observed reduction in the T_g of the nanocomposites may indicate weak or poor interactions between the polymer particles and CNCs, as previously reported by Meijouda et al. [68]. Except for NC5, which showed a sudden break in tensile testing, the breakage of the film of other nanocomposites did not occur instantly after the yield strength, and the nanocomposite films showed a resistance to break at one point (Figure 11). For instance, NC3 exhibited small initial cracks under tensile stress under both drying conditions but withstood additional stress in successive stages of cracking before ultimately breaking. The mechanical properties can be interpreted based on the drying rate. The highest drying rate of NC1–NC4 was reported for NC3. The faster drying rate of NC3 resulted in higher ultimate and yield strengths. Although Keddie [51] reported that faster drying caused films with less structure for the latexes, nanocomposites showed better mechanical properties at higher drying rates of the films.

The establishment of hydrogen bonds between hydroxyl groups on the surface of CNCs plays a crucial role in attaining high mechanical strength in cellulose nanocrystals [14, 69]. It was assumed that the formation of this network was governed by the percolation mechanism [14]. Percolation refers to the existence of a continuous path by the minor phase (percolating phase) within the major phase of a nanocomposite. The percolation threshold is the point at which percolation is achieved at the minimum concentration of the percolating phase. This condition defines continuous contact between the particles of the percolating phase throughout the entire product.

In our study, the establishment of hydrogen bonds between the cellulose nanocrystals was not achieved. The restriction on incorporating higher dosages of CNCs could be a reason for the lower mechanical properties of the nanocomposites.

4 | Conclusions

The semi-batch emulsion polymerization process successfully synthesized CNC and VA monomers as nanocomposites. The incorporation of CNC decelerated the drying rate of nanocomposite films and reduced the WVTR for moderate CNC loadings. Swelling tests confirmed improved film stability up to the maximum loading. Thermal analysis revealed reduced stability near 300°C but enhanced resistance below 250°C, indicating stabilizing interactions between the CNCs and polymer chains. All nanocomposites exhibited reduced ultimate strength and elongation at break, indicating increased brittleness; however, NC5 exhibited a higher elastic modulus than pristine PVAc, although the results displayed considerable fluctuations, as reflected by the large standard deviation. The nanocomposite films exhibited uneven surfaces with increasing CNC content, as observed under polarized microscopy. Microscopic analysis revealed the formation of mosaic-like surface patterns and enlarged particle domains with increasing CNC content, indicating restricted particle coalescence and heterogeneous film formation, which could contribute to the observed mechanical behavior. These findings emphasize the importance of optimizing the CNC loading for scalable nanocomposite applications.

Future optimization should focus on controlling processing parameters, particularly viscosity, to achieve controlled and optimized levels of CNC incorporation. Changing ingredients to bio-based and biodegradable ones enhances circularity and sustainability. Improving the filler-filler and filler-matrix interactions may further enhance the mechanical performance. Enabling improved mechanical properties and smoother film topography

while maintaining a lower WVTR presents an opportunity for future research.

Author Contributions

Shahab Nasr: conceptualization (lead), data curation (lead), formal analysis (lead), investigation (lead), methodology (lead), software (lead), validation (lead), visualization (lead), writing – original draft (lead), writing – review and editing (lead). **Pooria Khalili:** conceptualization (supporting), data curation (supporting), formal analysis (supporting), investigation (supporting), methodology (lead), supervision (supporting), validation (supporting), writing – review and editing (supporting). **Gunnar Westman:** conceptualization (supporting), resources (supporting), supervision (supporting). **Mikael Skrifvars:** conceptualization (supporting), funding acquisition (supporting), investigation (supporting), methodology (supporting), project administration (lead), resources (supporting), supervision (lead), writing – review and editing (supporting). **Fathi gouda:** methodology (supporting), supervision (supporting), investigation (supporting). **Juliana Aristéia de Lima:** methodology (lead), supervision (supporting), investigation (supporting).

Acknowledgments

The authors would like to thank our lab technicians Ville Skrifvars and Jonas Hansson for their technical support in conducting the experiments.

Funding

This research did not receive any external funding.

Ethics Statement

Not applicable.

Consent

All authors agree to publication.

Conflicts of Interest

The authors declare no conflicts of interest.

Data Availability Statement

Data will be available upon reasonable request.

References

1. T. Hassan, A. Salam, A. Khan, et al., "Functional Nanocomposites and Their Potential Applications: A Review," *Journal of Polymer Research* 28, no. 2 (2021).

2. N. Ayrilmis, E. Yurttas, E. Y. Avsar, et al., "Properties of Plastic Composites Filled With Giant Reed Flour and Magnesium Oxide Nanoparticles," *BioResources* 20, no. 2 (2025): 2670–2686.

3. P. R. Govindarajan, J. A. Antony, S. Palanisamy, N. Ayrilmis, H. Junaedi, and T. A. Sebaey, "Advances in Manufacturing of Carbon-Based Molecular Nanomaterials Based on Rice Husk/Hull Waste," *BioResources* 19, no. 4 (2024).

4. C. Miao, D. Mauran, and W. Y. Hamad, "How Hydrogen-Bonding Interactions and Nanocrystal Aspect Ratios Influence the Morphology and Mechanical Performance of Polymer Nanocomposites Reinforced With Cellulose Nanocrystals," *Soft Matter* 18, no. 24 (2022): 4572–4581.

5. K. Papapetros, G. N. Mathioudakis, D. Vroulias, N. Koutroumanis, G. A. Voyiatzis, and K. S. Andrikopoulos, "Structure-Properties Correlations of PVA-Cellulose Based Nanocomposite Films for Food Packaging Applications," *Polymers* 17, no. 14 (2025): 1911.

6. S. Nasr, P. Khalili, G. Westman, and M. Skrifvars, "Cellulose Nanocrystal–Reinforced Polyvinyl Acetate Nanolatex for Viscose Fabric Prepregs and Composite Materials," *Journal of Applied Polymer Science* 143, no. 7 (2026).

7. Y. Wang, B. Sun, Z. Hao, and J. Zhang, "Advances in Organic–Inorganic Hybrid Latex Particles via In Situ Emulsion Polymerization," *Polymers* 15, no. 14 (2023): 2995.

8. M. Anusuya, M. Meena, M. Durga, et al., "*Enhancement of Mechanical Performance on Polyethylene-Based Composites With Short Glass Fiber, Graphite Nano-Platelets, and Silicon Dioxide Nanoparticles*," in *AIP Conference Proceedings*, (AIP Publishing LLC, 2025).

9. W. Shanthi, G. Ramakrishna, M. Bakkiyaraj, et al., "Enhancement of Mechanical Properties in Hybrid Hemp-Epoxy Composites With Nano-Silicon Dioxide and Nanographene Fillers," in *AIP Conference Proceedings*, (AIP Publishing LLC, 2025).

10. A. S. Pakdel, E. Niinivaara, E. D. Cranston, R. M. Berry, and M. A. Dubé, "Cellulose Nanocrystal (CNC)–Latex Nanocomposites: Effect of CNC Hydrophilicity and Charge on Rheological, Mechanical, and Adhesive Properties," *Macromolecular Rapid Communications* 42, no. 3 (2021): 2000448.

11. S. Palanisamy, T. M. Murugesan, M. Palaniappan, C. Santulli, N. Ayrilmis, and A. Alavudeen, "Selection and Processing of Natural Fibers and Nanocellulose for Biocomposite Applications: A Brief Review," *BioResources* 19, no. 1 (2024).

12. M. A. S. Azizi Samir, F. Alloin, and A. Dufresne, "Review of Recent Research Into Cellulosic Whiskers, Their Properties and Their Application in Nanocomposite Field," *Biomacromolecules* 6, no. 2 (2005): 612–626.

13. A. P. Mathew, G. Gong, N. Bjorngrim, D. Wixe, and K. Oksman, "Moisture Absorption Behavior and Its Impact on the Mechanical Properties of Cellulose Whiskers-Based Polyvinylacetate Nanocomposites," *Polymer Engineering & Science* 51, no. 11 (2011): 2136–2142.

14. V. Favier, J. Y. Cavaille, G. R. Canova, and S. C. Shrivastava, "Mechanical Percolation in Cellulose Whisker Nanocomposites," *Polymer Engineering & Science* 37, no. 10 (1997): 1732–1739.

15. N. Ljungberg, C. Bonini, F. Bortolussi, C. Boisson, L. Heux, and J.-Y. Cavaillé, "New Nanocomposite Materials Reinforced With Cellulose Whiskers in Atactic Polypropylene: Effect of Surface and Dispersion Characteristics," *Biomacromolecules* 6, no. 5 (2005): 2732–2739.

16. L. Zhong, S. Fu, X. Peng, H. Zhan, and R. Sun, "Colloidal Stability of Negatively Charged Cellulose Nanocrystalline in Aqueous Systems," *Carbohydrate Polymers* 90, no. 1 (2012): 644–649.

17. J. M. Asua, "Emulsion Polymerization: From Fundamental Mechanisms to Process Developments," *Journal of Polymer Science Part A: Polymer Chemistry* 42, no. 5 (2004): 1025–1041.

18. C. Ordonez, M. A. Dube, and E. D. Cranston, "Enhancing the Properties of Latex-Based Coatings with Carboxylated Cellulose Nanocrystals," *Biomacromolecules* 26, no. 1 (2024): 480–489.

19. V. A. Gabriel, P. Champagne, M. F. Cunningham, and M. A. Dubé, "In-Situ Addition of Carboxylated Cellulose Nanocrystals in Seeded Semi-Batch Emulsion Polymerization," *The Canadian Journal of Chemical Engineering* 100, no. 4 (2022): 767–779.

20. S. A. Kedzior, V. A. Gabriel, M. A. Dubé, and E. D. Cranston, "Nanocellulose in Emulsions and Heterogeneous Water-Based Polymer Systems: A Review," *Advanced Materials* 33, no. 28 (2021): 2002404.

21. J. Sapkota, S. Kumar, C. Weder, and E. J. Foster, "Influence of Processing Conditions on Properties of Poly (Vinyl Acetate)/Cellulose Nanocrystal Nanocomposites," *Macromolecular Materials and Engineering* 300, no. 5 (2015): 562–571.

22. S. Geng, M. M.-U. Haque, and K. Oksman, "Crosslinked Poly (Vinyl Acetate)(PVAc) Reinforced With Cellulose Nanocrystals (CNC):

Structure and Mechanical Properties," *Composites Science and Technology* 126 (2016): 35–42.

23. A. P. Nozaki and L. M. Lona, "Comparison Between Cellulose Nanocrystal and Microfibrillated Cellulose as Reinforcement of Poly (Vinyl Acetate) Composites Obtained by Either In Situ Emulsion Polymerization or a Simple Mixing Technique," *Cellulose* 28, no. 4 (2021): 2273–2286.

24. S. Vineeth, R. V. Gadhave, and P. T. Gadekar, "Nanocellulose Applications in Wood Adhesives," *Open Journal of Polymer Chemistry* 9, no. 4 (2019): 63–75.

25. J. Meuldijk, M. F. Kemmere, S. V. W. De Lima, X. E. E. Reynhout, A. A. H. Drinkenburg, and A. L. German, "Some Key Factors in Emulsion Polymerization Process Development," *Polymer Reaction Engineering* 11, no. 3 (2007): 259–276.

26. T. A. Adams Ii and W. D. Seider, "Semicontinuous Reactive Distillation for Specialty Chemicals Production: Economic Comparison With Batch and Continuous Processing," in *AIChE Annual Meeting, Conference Proceedings*, (2005)

27. Y. H. Erbil, "Vinyl Acetate Emulsion Polymerization and Copolymerization With Acrylic Monomers," *CRC Press* 9 (2000).

28. M. S. El-Aasser, *Emulsion Polymerization of Vinyl Acetate* (Springer Science & Business, 2012).

29. J.-L. Gustin and F. Laganier, "Understanding Vinyl Acetate Polymerization Accidents," *Organic Process Research & Development* 9, no. 6 (2005): 962–975.

30. A. S. Pakdel, V. Gabriel, R. M. Berry, C. Fraschini, E. D. Cranston, and M. A. Dubé, "A Sequential Design Approach for In Situ Incorporation of Cellulose Nanocrystals in Emulsion-Based Pressure Sensitive Adhesives," *Cellulose* 27, no. 18 (2020): 10837–10853.

31. S. Mohebbi, R. A. Hutchinson, and M. F. Cunningham, "Exploring Bio-Based Monomers in Emulsion and Miniemulsion Polymerization," *Macromolecular Rapid Communications* 46, no. 12 (2025).

32. D. R. Bassett and A. E. Hamielec, *Emulsion Polymers and Emulsion Polymerization* (ACS Publications, 1981).

33. R. J. Moon, A. Martini, J. Nairn, J. Simonsen, and J. Youngblood, "Cellulose Nanomaterials Review: Structure, Properties and Nanocomposites," *Chemical Society Reviews* 40, no. 7 (2011): 3941–3994.

34. J. Araki, M. Wada, S. Kuga, and T. Okano, "Flow Properties of Microcrystalline Cellulose Suspension Prepared by Acid Treatment of Native Cellulose," *Colloids and Surfaces A: Physicochemical and Engineering Aspects* 142, no. 1 (1998): 75–82.

35. A. Chakrabarty and Y. Teramoto, "Recent Advances in Nanocellulose Composites With Polymers: A Guide for Choosing Partners and How to Incorporate Them," *Polymers* 10, no. 5 (2018): 517.

36. C. Miao and W. Y. Hamad, "Cellulose Reinforced Polymer Composites and Nanocomposites: A Critical Review," *Cellulose* 20, no. 5 (2013): 2221–2262.

37. S. Camarero Espinosa, T. Kuhnt, E. J. Foster, and C. Weder, "Isolation of Thermally Stable Cellulose Nanocrystals by Phosphoric Acid Hydrolysis," *Biomacromolecules* 14, no. 4 (2013): 1223–1230.

38. X. M. Dong, J.-F. Revol, and D. G. Gray, "Effect of Microcrystallite Preparation Conditions on the Formation of Colloid Crystals of Cellulose," *Cellulose* 5, no. 1 (1998): 19–32.

39. M. Labet and W. Thielemans, "Improving the Reproducibility of Chemical Reactions on the Surface of Cellulose Nanocrystals: ROP of ε-Caprolactone as a Case Study," *Cellulose* 18, no. 3 (2011): 607–617.

40. C. Fritz and J. F. Olivera, "Nanocellulose in Heterogeneous Water-Based Polymerization for Wood Adhesives," *Polysaccharides* 3, no. 1 (2022): 219–235.

41. C. E. Meree, G. T. Schueneman, J. C. Meredith, and M. L. Shofner, "Rheological Behavior of Highly Loaded Cellulose Nanocrystal/Poly (Vinyl Alcohol) Composite Suspensions," *Cellulose* 23, no. 5 (2016): 3001–3012.

42. N. El Miri, K. Abdelouahdi, M. Zahouily, et al., "Bio-Nanocomposite Films Based on Cellulose Nanocrystals Filled Polyvinyl Alcohol/Chitosan Polymer Blend," *Journal of Applied Polymer Science* 132, no. 22 (2015).

43. M. El Achaby, N. E. Miri, A. Aboulkas, et al., "Processing and Properties of Eco-Friendly Bio-Nanocomposite Films Filled With Cellulose Nanocrystals From Sugarcane Bagasse," *International Journal of Biological Macromolecules* 96 (2017): 340–352.

44. S. Carra, A. Sliepcevich, A. Canevarolo, and S. Carrà, "Grafting and Adsorption of Poly (Vinyl) Alcohol in Vinyl Acetate Emulsion Polymerization," *Polymer* 46, no. 4 (2005): 1379–1384.

45. N. Kim, E. D. Sudol, V. L. Dimonie, and M. S. El-Aasser, "Poly (Vinyl Alcohol) Stabilization of Acrylic Emulsion Polymers Using the Miniemulsion Approach," *Macromolecules* 36, no. 15 (2003): 5573–5579.

46. L. Qiao, A. J. Easteal, C. J. Bolt, P. K. Coveny, and R. A. Franich, "Improvement of the Water Resistance of Poly (Vinyl Acetate) Emulsion Wood Adhesive," *Pigment & Resin Technology* 29, no. 3 (2000): 152–158.

47. N. Kim, E. D. Sudol, V. L. Dimonie, and M. S. El-Aasser, "Comparison of Conventional and Miniemulsion Copolymerizations of Acrylic Monomers Using Poly (Vinyl Alcohol) as the Sole Stabilizer," *Macromolecules* 37, no. 7 (2004): 2427–2433.

48. S. Wohlhauser, G. Delepierre, M. Labet, et al., "Grafting Polymers From Cellulose Nanocrystals: Synthesis, Properties, and Applications," *Macromolecules* 51, no. 16 (2018): 6157–6189.

49. J. Tang, M. F. X. Lee, W. Zhang, B. Zhao, R. M. Berry, and K. C. Tam, "Dual Responsive Pickering Emulsion Stabilized by Poly [2-(Dimethylamino) Ethyl Methacrylate] Grafted Cellulose Nanocrystals," *Biomacromolecules* 15, no. 8 (2014): 3052–3060.

50. P. Mischke, *Film Formation: in Modern Paint Systems* (Vincentz, 2019).

51. J. L. Keddie, "Film Formation of Latex," *Materials Science and Engineering: R: Reports* 21, no. 3 (1997): 101–170.

52. H.-J. Butt and B. Gerharz, "Imaging Homogeneous and Composite Latex Particles With an Atomic Force Microscope," *Langmuir* 11, no. 12 (1995): 4735–4741.

53. E. Bradford and J. Vanderhoff, "Additional Studies of Morphological Changes in Latex Films," *Journal of Macromolecular Science, Part B: Physics* 6, no. 4 (2006): 671–693.

54. J. Keddie and A. F. Routh, *Fundamentals of Latex Film Formation: Processes and Properties* (Springer, 2010).

55. P. A. Lovell and M. S. El-Aasser, *Emulsion Polymerization and Emulsion Polymers* (Wiley, 1997).

56. I. C. McNeill, S. Ahmed, and L. Memetea, "Thermal Degradation of Vinyl Acetate—Methacrylic Acid Copolymer and Homopolymers. I. An FTIR Spectroscopic Investigation of Structural Changes in the Degrading Material," *Polymer Degradation and Stability* 47, no. 3 (1995): 423–433.

57. A. Ballistreri, S. Foti, G. Montaudo, and E. Scamporrino, "Evolution of Aromatic Compounds in the Thermal Decomposition of Vinyl Polymers," *Journal of Polymer Science: Polymer Chemistry Edition* 18, no. 4 (1980): 1147–1153.

58. B. J. Holland and J. N. Hay, "The Thermal Degradation of Poly (Vinyl Acetate) Measured by Thermal Analysis–Fourier Transform Infrared Spectroscopy," *Polymer* 43, no. 8 (2002): 2207–2211.

59. H. B. Yamak, "Emulsion Polymerization: Effects of Polymerization Variables on the Properties of Vinyl Acetate Based Emulsion Polymers," *Polymer Science* 5 (2013): 35–72.

60. E. E. Kiziltas, A. Kiziltas, S. C. Bollin, and D. J. Gardner, "Preparation and Characterization of Transparent PMMA–Cellulose-Based Nanocomposites," *Carbohydrate Polymers* 127 (2015): 381–389.

61. N. Girouard, G. T. Schueneman, M. L. Shofner, and J. C. Meredith, "Exploiting Colloidal Interfaces to Increase Dispersion, Performance, and Pot-Life in Cellulose Nanocrystal/Waterborne Epoxy Composites," *Polymer* 68 (2015): 111–121.

62. N. Wang, E. Ding, and R. Cheng, "Thermal Degradation Behaviors of Spherical Cellulose Nanocrystals With Sulfate Groups," *Polymer* 48, no. 12 (2007): 3486–3493.

63. P. Gan, S. Sam, MFb Abdullah, and M. F. Omar, "Thermal Properties of Nanocellulose-Reinforced Composites: A Review," *Journal of Applied Polymer Science* 137, no. 11 (2020): 48544.

64. J. Kim, G. Montero, Y. Habibi, et al., "Dispersion of Cellulose Crystallites by Nonionic Surfactants in a Hydrophobic Polymer Matrix," *Polymer Engineering & Science* 49, no. 10 (2009): 2054–2061.

65. E. Limousin, N. Ballard, and J. M. Asua, "Synthesis of Cellulose Nanocrystal Armored Latex Particles for Mechanically Strong Nanocomposite Films," *Polymer Chemistry* 10, no. 14 (2019): 1823–1831.

66. E. Limousin, I. Rafaniello, T. Schäfer, N. Ballard, and J. M. Asua, "Linking Film Structure and Mechanical Properties in Nanocomposite Films Formed From Dispersions of Cellulose Nanocrystals and Acrylic Latexes," *Langmuir* 36, no. 8 (2020): 2052–2062.

67. Z. W. Abdullah, Y. Dong, I. J. Davies, and S. Barbhuiya, *PVA Blends, and Their Nanocomposites for Biodegradable Packaging Application* (Polymer-Plastics Technology and Engineering, 2017): 1307–1344.

68. A. Meijouda, M. Chaari, H. Kaddami, et al., "Dielectric Properties and Molecular Dynamics of Cellulose Nanocrystal-Reinforced Polyvinyl Acetate Bio-Nanocomposites," *Journal of Molecular Liquids* 437 (2025): 128497.

69. V. Favier, G. R. Canova, J. Y. Cavaillé, H. Chanzy, A. Dufresne, and C. Gauthier, "Nanocomposite Materials From Latex and Cellulose Whiskers," *Polymers for Advanced Technologies* 6, no. 5 (1995): 351–355.